Check for updates

Global Biogeochemical Cycles

RESEARCH ARTICLE
10.1029/2020GB006541

Key Points:
- Solute concentrations are controlled significantly by the fluid transit time and reactivity
- Globally, carbonate weathering plays a controlling role in HCO_3^- spatial distributions and temporal dynamics
- Climate-weathering feedback is strong in Chinese rivers, because of the near-thermodynamic limit of HCO_3^-

Supporting Information:
- Supporting Information S1

Correspondence to:
S.-L. Li,
siliang.li@tju.edu.cn

Citation:
Zhong, J., Li, S.-L., Ibarra, D. E., Ding, H., & Liu, C.-Q. (2020). Solute production and transport processes in Chinese monsoonal rivers: Implications for global climate change. *Global Biogeochemical Cycles*, *34*, e2020GB006541. https://doi.org/10.1029/2020GB006541

Received 16 JAN 2020
Accepted 13 AUG 2020
Accepted article online 24 AUG 2020

©2020. American Geophysical Union. All Rights Reserved.

Solute Production and Transport Processes in Chinese Monsoonal Rivers: Implications for Global Climate Change

Jun Zhong[1], Si-Liang Li[1], Daniel E. Ibarra[2,3], Hu Ding[1], and Cong-Qiang Liu[1,4]

[1]Institute of Surface-Earth System Science, School of Earth System Science, Tianjin University, Tianjin, China, [2]Department of Geological Sciences, Stanford University, Stanford, CA, USA, [3]Department of Earth and Planetary Science, University of California, Berkeley, CA, USA, [4]State Key Laboratory of Environmental Geochemistry, Institute of Geochemistry, Chinese Academy of Sciences, Guiyang, China

Abstract The negative feedback between chemical weathering and climate is hypothesized to act as an important control on modulating atmospheric CO_2 over geologic timescales, affecting the evolution of Earth's climate over the history of Earth. Here, we investigated solute production processes by analyzing concentration-discharge, denoted here as concentration-runoff (*C*-*q*), relationships of Chinese monsoonal rivers, through both the empirical power law relationship and a recently developed Solute Production Model. We found that solute concentrations were highly modulated by hydrologic conditions which shifted the Damköhler number, *Da*, the ratio of fluid transit time versus the time required to reach equilibrium. Additionally, the among-catchment behavior of HCO_3^- responding to changing runoff was correlated with the average *Da* of each catchment. Rivers with high average *Da* induced high maximum weathering fluxes, while the maximum weathering potential was primarily controlled by the Damköhler coefficient (*Dw*, m/yr), the reactivity of the material in the weathering zone over a given length scale, among the catchments in this study. Globally, HCO_3^- behaviors and weathering characteristics are highly influenced by carbonate bedrock distributions and abundance. In addition, Chinese monsoonal rivers have higher weathering fluxes, weathering potential, and climate-weathering feedback sensitivity (4.4%/°C) than most other global rivers. Our work disclosed the mechanisms that link runoff, lithology, and weathering fluxes in monsoonal rivers and analyzed the controlling factors on solute dynamics on global scale, which can be implemented in exploring the chemical weathering processes under ongoing global climate change.

Plain Language Summary Continental weathering controls many aspects of the surface-Earth system, including imposing negative feedback on long-term carbon cycle. In this study, empirical power law relationship and process-based Solute Production Model (*SPM*) were used to disclose solute production and transport processes based on temporal sampling and analyses from Chinese monsoonal rivers. We found that high dissolution rates and high reactive surface areas led to solute concentrations that were relatively invariant with changing runoff. Additionally, the among-catchment behavior of HCO_3^- responding to changing runoff was correlated with the average ratio of fluid transit time versus the time required to reach equilibrium of each catchment. Globally, the areal proportion of carbonate controls the HCO_3^- dynamics and weathering potential. The climate-weathering feedback sensitivity is 4.4%/°C for Chinese rivers, which is much stronger than the global average sensitivity of 3.6%/°C, based on the *SPM*. In this work we demonstrated that the solute transport fluxes of Chinese monsoonal rivers will be more sensitive to hydrologic variabilities than most other global rivers under ongoing anthropogenic global climate change. Our conclusions highlighted chemical weathering processes under various hydrologic conditions and illustrated how chemical concentration patterns and weathering fluxes may change under global climate change in rivers worldwide.

1. Introduction

Continental weathering controls many aspects of the surface-Earth system. This includes imposing negative feedback on the geologic carbon cycle (e.g., Berner et al., 1983; Walker et al., 1981; West, 2012; Winnick & Maher, 2018), shaping the Earth's surface as a component of denudation (Dixon et al., 2012; West et al., 2005), and transferring chemical species from the land to the oceans (Amiotte Suchet et al., 2003; Gaillardet

et al., 1999; Stallard & Edmond, 1981), and in doing so it helps regulate the Earth's climate over geologic time (e.g., Berner & Caldeira, 1997; Caves Rugenstein et al., 2019; Maher & Chamberlain, 2014). Numerous studies have shown that chemical weathering fluxes are sensitive to multiple climate variables, such as runoff (q, defined herein as discharge [Q]/drainage area [A], also sometimes described as specific discharge), precipitation, and temperature (e.g., Gaillardet et al., 1999; Goudie & Viles, 2012; Ibarra et al., 2016; Li et al., 2016; Zhong et al., 2018). Consequently, the interplay between climate variabilities and chemical weathering reactions in catchment systems acts as an important control in shaping the Earth's surface carbon cycle (e.g., Maher & Chamberlain, 2014; Winnick & Maher, 2018; Zhong et al., 2018). Hydrologic regulations are proved as a critically important driver of chemical weathering fluxes, as they shift chemical weathering fluxes by changing the reactive surface area and influencing the rate at which the dissolved loads in waters approach thermodynamic equilibrium (Ibarra et al., 2016; Maher, 2010, 2011; Raymond, 2017; West et al., 2005). Importantly, the role of hydrology on chemical weathering is thus readily apparent from measurements of major ions, derived primarily from chemical weathering reactions, in the form of concentration-discharge relationships, which rarely show simple dilution with increasing runoff. Rather, many ions show close to "chemostatic" behavior (i.e., constant concentration with changing runoff) (Godsey et al., 2009; Ibarra et al., 2016, 2017; Moon et al., 2014; Zhong, Li, Tao, Yue, et al., 2017).

Given these past advances in our understanding of the processes involved, further understanding the control of hydrological processes on water chemistry and the source of measured chemical species is imperative for understanding the effects of future changing climate on chemical weathering (Bhatt et al., 2018; Hunsaker & Johnson, 2017) and applying these relationships to our understanding of the geologic carbon cycle over the history of the Earth (Ibarra et al., 2016; Maher & Chamberlain, 2014; von Blanckenburg et al., 2015). Previous work has demonstrated that concentration-discharge relationships, denoted herein as concentration-runoff (C-q), varies substantially between different elements (Ibarra et al., 2016; Torres et al., 2015; Zhong, Li, Tao, Yue, et al., 2017), different catchments (Musolff et al., 2017; Wymore et al., 2017), and over different timescales (Joesoef et al., 2017), providing insights into physical, chemical, and biological processes controlling C-q relationships (Clow & Mast, 2010; Thompson et al., 2011; Torres et al., 2015). Consequently, investigating the C-q relationships for various elements on multiple spatial and temporal scales may provide important inferences for understanding the controls of lithology and climate on chemical weathering (Baronas et al., 2017; Ibarra et al., 2016; Maher & Chamberlain, 2014; Torres et al., 2015; Zhong et al., 2018).

Chinese rivers show higher weathering rates than most other global rivers (Gaillardet et al., 1999), and monsoonal climate induces asymmetric seasonal precipitation in the Chinese monsoonal regions. Therefore, chemical weathering processes in Chinese river basins are affected by a complex suite of Earth surface process (e.g., hydrological process). However, the effects of hydrologic variabilities on chemical weathering and the controlling mechanisms in Chinese monsoonal regions remain unclear. This study used a process-based Solute Production Model (*SPM*) (Ibarra et al., 2016; Maher & Chamberlain, 2014; Wymore et al., 2017) and empirical power law relationships (Godsey et al., 2009; Torres et al., 2015; Zhong et al., 2018) for investigating the solutes' dynamics in Chinese monsoonal rivers that may explain the response of chemical weathering processes to various hydrologic conditions for monsoonal rivers. This study was conducted to evaluate (1) the nature and causes of major ions' C-q relationships for monsoonal rivers, (2) the controlling factors (i.e., lithology and runoff) of chemical weathering for different rivers, and (3) the potential climate-weathering feedback sensitivity to global climate change and the controlling mechanisms.

2. Material and Methods

2.1. Site Descriptions and Data Sources

The three river basins considered in this study are the Yellow River (YR), the Changjiang River (CR), and the Pearl River (PR). We also compared these data to results from the global rivers data set reported by Ibarra et al. (2017) and Moon et al. (2014). In this study, the outlets of the YR (Lijin station, YR @ Lijin), the CR (Datong station, CR @ Datong), and site at the middle mainstream of the CR (Qingxi station, CR @ Qingxi) were sampled, and major ions were analyzed in this study (Figure 1a, red circles), the methods of which were the same as those of Zhong, Li, Tao, Ding, et al. (2017). Published data sets of other sites in

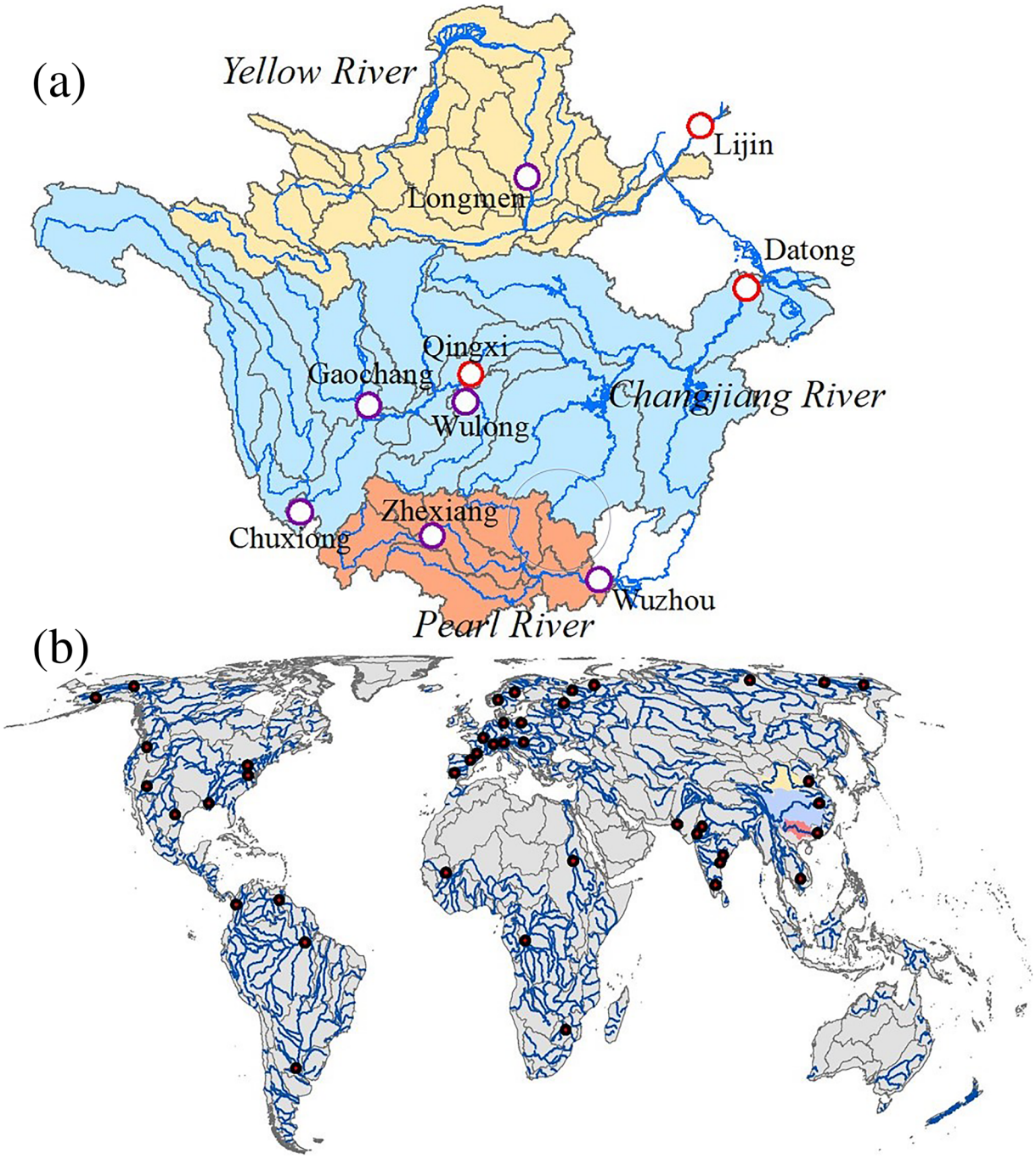

Figure 1. Maps of sites in this analysis. (a) The red circles represent the data sets of sampling in this study, and the purple circles are from compilations of others' study. (b) Sites of analyses of the global rivers data set from Ibarra et al. (2017) and Moon et al. (2014).

these three river basins were compiled from previous studies (Figure 1a, purple circles), which included Longmen station at the YR (YR @ Longmen, Zhang et al., 2015), Chuxiong station at the Longchuan River (Li et al., 2011), Gaochang station at the Min River (Zhong, Li, Tao, Ding, et al., 2017), Wulong station at the Wujiang River (Zhong, Li, Tao, Yue, et al., 2017), Zhexiang station at the Hongshui River (Liu et al., 2017), and Wuzhou station at the PR (PR @ Wuzhou, Zhong et al., 2018).

The sampling regime for the study rivers presented here included time series sampling over the following: YR @ Lijin (February 2015 to February 2016; $n = 16$), CR @ Datong (January 2015 to February 2016;

$n = 22$), CR @ Qingxi (January 2015 to February 2016; $n = 15$), YR @ Longmen (January 2013 to December, 2013; $n = 60$), Longchuan River (September 2007 to August 2009; $n = 48$), Min River (November 2013 to October 2014; $n = 27$), Wujiang River (November 2013 to October 2014; $n = 34$), Hongshui River (October 2013 to September 2014; $n = 12$), and PR @ Wuzhou (October 2013 to September 2014; $n = 38$). The lithological and climatic details of these sites analyzed in this study were described in the supporting information.

2.2. Methods: Power Law Fitting and *SPM*

In order to express the temporal variabilities of solutes in the river system, the ratio of coefficient of solute concentration variations versus runoff variations are implemented (Musolff et al., 2017; Thompson et al., 2011; Zhong et al., 2018) as

$$CV_C/CV_q = \left(\mu_q/\mu_C\right) \times \left(\delta_C/\delta_q\right) \tag{1}$$

which is derived from mean (μ) and standard deviation (δ). In the case of chemostatic behavior, CV_C/CV_q would be near to 0 (Musolff et al., 2017). Power law fitting of *C*-*q* relationships was revived by Godsey et al. (2009) by analyzing the data of small basins in the U.S. Hydrology Benchmark Network.

$$C_i\ (\text{solute concentration}) = a \times (q_i\ (\text{runoff}))^b \tag{2}$$

where a and b are constants. Because solutes' concentrations always do not keep pace with water flow, the power law exponent (b) can be used to express the solutes' behaviors in response of hydrologic changes (Rose, 2003; Wymore et al., 2017). When b is near to 0 (i.e., $-0.2 < b < 0.2$), the solute would display chemostatic behavior responding to the changing runoff (Godsey et al., 2009; Torres et al., 2015; Wymore et al., 2017). Particularly, when b is 0, solute would behave totally chemostatically; that is, the solutes keep concentrations constant as runoff changes. Positive b values (i.e., $b > 0.2$) are defined as displaying enrichment behavior, and negative b values (i.e., $b < -0.2$) are defined as displaying dilution behavior (i.e., source limited) (Godsey et al., 2009; Zhong et al., 2018). In addition, b value of -1 would indicate that solute's concentrations change inversely with discharge; that is, approximately constant fluxes of solutes are diluted by increasing fluxes of water.

In order to decipher the complex weathering processes, the *SPM* was newly proposed by Maher and Chamberlain (2014) based on the solute production equation. The model links weathering processes to both the reactivity of the weathering zone and the specific runoff, as well as the fluid transit time distribution through a given catchment (Maher & Chamberlain, 2014; Wymore et al., 2017), which is shown as

$$C = C_0/(1 + Dw/q) + C_{max} \times (Dw/q)/(1 + Dw/q) \tag{3}$$

where C_0 is the initial solute concentration, Dw (m/yr) is the Damköhler coefficient, and C_{max} is the theoretical maximum solute concentration, impacted by a "thermodynamic limit," all of which are estimated by nonlinear fitting of C and q (Ibarra et al., 2016; Maher & Chamberlain, 2014; Wymore et al., 2017). Note that here we followed Ibarra et al. (2016) and used the version of the *SPM* that did not include the exponential scaling factor used in Maher and Chamberlain (2014). C_0 is the initial solute concentration, which is derived from atmospheric deposition and hydrothermal or deep groundwater inputs and is independent of runoff (Ibarra et al., 2016; Wymore et al., 2017). For most catchments, the C_0 is assumed to be 0, so Equation 1 can be simplified as below:

$$C = C_{max} \times (Dw/q)/(1 + Dw/q) = C_{max} \times Dw/(q + Dw) \tag{4}$$

The analyses of *C*-*q* relationships were carried out in this study to derive the Dw and C_{max} values using time series (at least 1 year) data set on individual sample sites (e.g., Ibarra et al., 2016, 2017; Wlostowski et al., 2018; Wymore et al., 2017). A nonlinear least squares fitting was applied in this study to derive the Dw and C_{max} values by using the Gauss-Newton algorithm (*nls2*-function of program *R*) (CRAN, 2018; Grothendieck, 2013), used by modifying the *R* scripts published by Ibarra et al. (2016). The Gauss-Newton method successively iterated the estimate to minimize the square of errors between

the model prediction and the input data set that produces the best fit by optimization (Bhatt et al., 2018; Ibarra et al., 2016).

Within the solute production modeling framework, Damköhler number (Da), a dimensionless number, represents the ratio of the fluid travel time (T_f [yr]) versus the time required to reach equilibrium (T_{eq} [yr]) (Ibarra et al., 2016; Maher, 2010, 2011; Maher & Chamberlain, 2014; Wlostowski et al., 2018):

$$Da = T_f/T_{eq} = R_n \times L \times \Phi/(q \times C_{max}) \tag{5}$$

where R_n (μmol/L) is the net mineral dissolution rate, L (m) is the flowpath length, Φ is the effective porosity, and L being multiplied by Φ represents the reactive flowpath length ($L\Phi$) (Ibarra et al., 2016; Wlostowski et al., 2018). Theoretically, when $Da > 1$, T_f is longer than T_{eq}, implying that the reactivity of weathering zone controls the solute concentrations (Ibarra et al., 2016; Maher, 2010, 2011; Maher & Chamberlain, 2014; Wlostowski et al., 2018). Da can be driven by changes in travel time or equilibrium time; thus, Da is nonunique in a certain catchment. As Dw was defined as $Dw = L \times \Phi/T_{eq}$, Da ($Da = Dw/q$) can be calculated from the fitted Dw values of sampling sites and the given specific runoff conditions for each sample. Equation 3 can thus be simplified as (see derivation in Maher and Chamberlain (2014)):

$$C = C_{max} \times (Da)/(1 + Da) \tag{6}$$

Theoretically, when Da is equal to 1, the T_f is enough to saturate and equal to T_{eq}, and q approaches Dw. When the Da value is higher than 1, this thereby indicates that T_f is much longer than T_{eq} (Wlostowski et al., 2018). In the calculation, the T_f means the average transit time (Maher & Chamberlain, 2014), and T_f must be much higher than T_{eq} by a factor of approximately 15 for a C-q relationship to be chemostatic (Ibarra et al., 2016). In reality, T_f in the large catchment represents an ensemble of water travel times which can be represented by a probability density function (*pdf*) (Maher & Chamberlain, 2014). For the derivation of the *SPM* model, Maher and Chamberlain (2014) used the travel time *pdfs* to describe the movement of water and solutes in large catchments, without the need to specify the spatial hydrologic and morphological heterogeneity (Maher & Chamberlain, 2014). Although the detailed patterns of the catchments are not known, the stochastic representation of travel times has the advantage of working in heterogeneous catchments (von Blanckenburg et al., 2015; Blöschl & Sivapalan, 1995; Maher & Chamberlain, 2014). Therefore, the *SPM* model can be used in large catchments (details of derivation in supplementary materials of Maher & Chamberlain, 2014).

2.3. Chemical Weathering Calculations

The weathering fluxes are calculated from C by multiplying by q ($WF = q \times C$, ton/km^2/yr), which can be modified as

$$WF = q \times C_{max} \times (Dw/q)/(1 + Dw/q) = q \times C_{max} \times Da/(1 + Da) \tag{7}$$

Higher Dw and C_{max} values result in a higher theoretical maximum weathering fluxes (WF_{max}) value, which can be calculated through $WF_{max} = Dw \times C_{max}$, indicating water spending sufficient time to reach equilibrium with minerals (Ibarra et al., 2016; Maher & Chamberlain, 2014). For a given mean observed WF (WF_{obs}), we can calculate the normalized weathering intensity:

$$NWI = WF_{obs} \times 100\%/WF_{max} = 100\%/(1 + Da) \tag{8}$$

For a given mean WF_{obs}, the difference between WF_{max} and WF_{obs} was defined as the absolute weathering potential of a catchment ($\Delta WP = WF_{max} - WF_{obs}$). The normalized weathering potential (WP_{norm}) is used to represent the future weathering potential under ongoing climate change (Ibarra et al., 2016), which is defined as

$$WP_{norm} = \Delta WP \times 100/WF_{max} = (WF_{max} - WF_{obs}) \times 100/WF_{max} \quad (9)$$

3. Results

3.1. Runoff Characteristics and Spatial Variations of Major Ions

The runoff values for the data sets analyzed here, in decreasing order were Wujiang River > PR @ Wuzhou > Minjiang River > CR @ Datong > Hongshui River > CR @ Qingxi > Longchuan River > YR @ Longmen > YR @ Lijin (Table 1). Higher runoff was observed in rivers located in south China, such as the Wujiang River, PR @ Wuzhou, and the Min River (Table 1 and Figure 1). The basins in the CR and the PR showed high runoff with large seasonal variations (Table 1). Contrarily, the runoff in the two stations of the YR was the lowest in these analyzed sites (Table 1).

Mean flow-weighted concentration (C_W), which was defined as $\sum(q_i \times C_i)/\sum q_i$ (Godsey et al., 2009; Hunsaker & Johnson, 2017), was used here to express the solute concentrations normalized by the variations in hydrologic conditions. For the Na^+, the highest C_W was observed in YR @ Lijin (4,491 μmol/L), followed by YR @ Longmen (3,971 μmol/L), both of which were located in the YR (Table 1). The lowest C_W of Na^+ was observed in the PR @ Wuzhou (100 μmol/L, Table 1), whose characteristics were similar to Cl^-. Compared with Na^+, the C_W of HCO_3^- and Ca^{2+} in these rivers varied in a narrow range, from 1,576 to 3,489 μmol/L and from 824 to 1,538 μmol/L, respectively (Table 1). The highest C_W values of HCO_3^-, Ca^{2+} and Mg^{2+} were observed in YR @ Longmen and Lijin, and Wujiang River showed the lowest C_W values (Table 1). For K^+, the highest C_W value was observed in the Longchuan River, which was twice of that in YR @ Longmen and Lijin, and fourfold to fivefold of other sites (Table 1). Finally, the C_W values of SO_4^{2-} in YR @ Longmen and Lijin showed the highest values, followed by the Wujiang River and the Hongshui River, with the lowest value in the PR @ Wuzhou (Table 1).

3.2. Temporal Variations of Major Ions and *C-q* Relationships (Power Law and *SPM* Fits)

HCO_3^-, Mg^{2+}, and Ca^{2+} showed the lowest CV_C/CV_q ratios (Table 1), with the CV_C/CV_q ratios of HCO_3^- varying from 0.05 in the Wujiang River of karst areas to 0.38 in YR @ Longmen (Table 1). The lowest CV_C/CV_q ratio of Ca^{2+} was observed in YR @ Lijin, and the highest value occurred in the Wujiang River, similar to Mg^{2+} (Table 1). For the Na^+ and Cl^-, although the CV_C/CV_q ratios in most sites had higher ratios (Table 1), these ratios in YR @ Lijin showed lower values. The CV_C/CV_q ratios of K^+ varied in a narrow range, from 0.16 to 0.31, except in the PR @ Wuzhou (0.53) (Table 1). PR @ Wuzhou had the highest SO_4^{2-}-CV_C/CV_q ratio of 0.61, and others showed similar CV_C/CV_q ratios, besides YR @ Lijin which showed the lowest value (Table 1).

Most ions showed significant temporal variations, with higher concentrations during low-flow (base-flow) seasons and lower values during high-flow seasons (Figure 2). The *C-q* fits of Ca^{2+}+Mg^{2+}, Na^+, HCO_3^-, and total dissolved solids (TDS) for all the catchments compiled in this study were reported in Table 2, and power law fitting and *SPM* were used in this study. The *b* values of Ca^{2+}+Mg^{2+} ranged from −0.19 to −0.041, and *b* values of HCO_3^- varied from −0.20 to −0.030, with the lowest value for both HCO_3^- and Ca^{2+}+Mg^{2+} occurring in YR @ Lijin (Table 2). The *b* values of Na^+ varied from −0.48 to −0.058, with the lowest and highest values located in CR @ Datong and YR @ Lijin, respectively (Table 2). TDS showed similar *b* value ranges as Ca^{2+}+ Mg^{2+}, varying from −0.19 to −0.045 (Table 2). The C_{max} values from the *SPM* showed similar trend as the *Cw* values for the complied catchments (Table 2), and the highest values were observed in the locations of the YR. The Ca^{2+}+Mg^{2+}, HCO_3^-, and TDS had wide *Dw* values, with the *Dw* values ranges of 0.40 to 20.73, 0.22 to 47.26, and 0.42 to 18.37, respectively (Table 2). And for Ca^{2+}+Mg^{2+}, HCO_3^-, and TDS, the lowest *Dw* values were observed in the YR @ Longmen, and the highest *Dw* values occurred in Wujiang River (Table 2). But the *Dw* values of Na^+ had a narrower range, from 0.42 to 2.56 (Table 2). Goodness of fit criteria analyzing residuals showed that the root-mean-square error (RMSE) values for the *SPM* and power law fits are similar for all these solutes (supporting information Table S1). Based on the *SPM*, the HCO_3^--WF_{max} values could be calculated, ranging from 1.02×10^6 to 119.19×10^6 mol/km^2/yr for these Chinese monsoonal rivers, with the lowest and the highest value occurring in YR @ Longmen and Wujiang River, respectively.

Table 1
The Characteristics of Runoff and Major Ions of the Chinese Monsoonal Rivers

	Runoff (m/yr)		Ca^{2+} (μmol/L)		Mg^{2+} (μmol/L)		Na^{+} (μmol/L)		K^{+} (μmol/L)		HCO_3^{-} (μmol/L)		SO_4^{2-} (μmol/L)		Cl^{-} (μmol/L)		Lithology
Sampling sites	Min	Max	*Cw*	CV_C/CV_q	*Cw*	CV_C/CV_q	*Cw*	CV_C/CV_q	*Cw*	CV_C/CV_q	*Cw*	CV_C/CV_q	*Cw*	CV_C/CVq	*Cw*	CV_C/CV_q	Carbonates proportion
Yellow River (YR)																	
YR @l ongmen	0.011	0.15	1,538	0.29	1,220	0.28	3,972	0.31	107	0.20	3,498	0.38	1,419	0.30	2,619	0.39	0.21
YR @ lijin	0.0046	0.12	1,427	0.05	1,171	0.12	4,491	0.12	102	0.16	3,272	0.11	1700	0.07	2,998	0.13	0.29
Changjiang River (CR)																	
CR @ datong	0.31	1.45	918	0.25	292	0.31	431	0.65	58	0.31	1740	0.15	325	0.36	320	0.69	0.44
Min River	0.28	2.26	939	0.13	321	0.35	304	0.62	52	0.23	1920	0.12	302	0.33	180	0.57	0.38
CR @ qingxi	0.16	0.99	1,117	0.15	409	0.15	547	0.32	57	0.23	2,190	0.09	429	0.21	374	0.38	0.50
Wujiang River	0.13	5.42	1,335	0.11	396	0.14	167	0.43	41	0.17	2,393	0.05	446	0.27	126	0.40	0.98
Longchuan River	0.0132	1	1,232	0.17	244	0.20	495	0.21	208	0.29	2,868	0.10	294	0.17	225	0.27	0.32
Pearl River (PR)																	
PR @ wuzhou	0.165	2.35	824	0.41	168	0.46	100	0.78	38	0.53	1,576	0.37	142	0.61	104	0.55	0.67
Hongshui River	0.3	1.49	1,072	0.23	455	0.19	240	0.43	47	0.22	2,276	0.28	429	0.32	145	0.29	0.87

4. Discussion

4.1. Drivers of the *C-q* Relationships

Various ions showed different behaviors responding to changing runoff conditions, and the same ion among different catchments displayed different behaviors in response of runoff changes, both of which can be identified by CV_C/CV_q ratios, *b* and *Dw* values (Tables 1 and 2; Figure 2). Spatial and temporal variations of major ion concentrations and relevant fluxes are usually associated with differing hydrologic and lithological conditions (Ibarra et al., 2016; Torres et al., 2015; Wymore et al., 2017). Significant spatial heterogenicities of various *C-q* relationships for the nine sites of Chinese monsoonal rivers were observed in this study (Figure 2). Due to the abundance of loess deposits in arid and semiarid climates (Chen et al., 2005), most ions in the YR

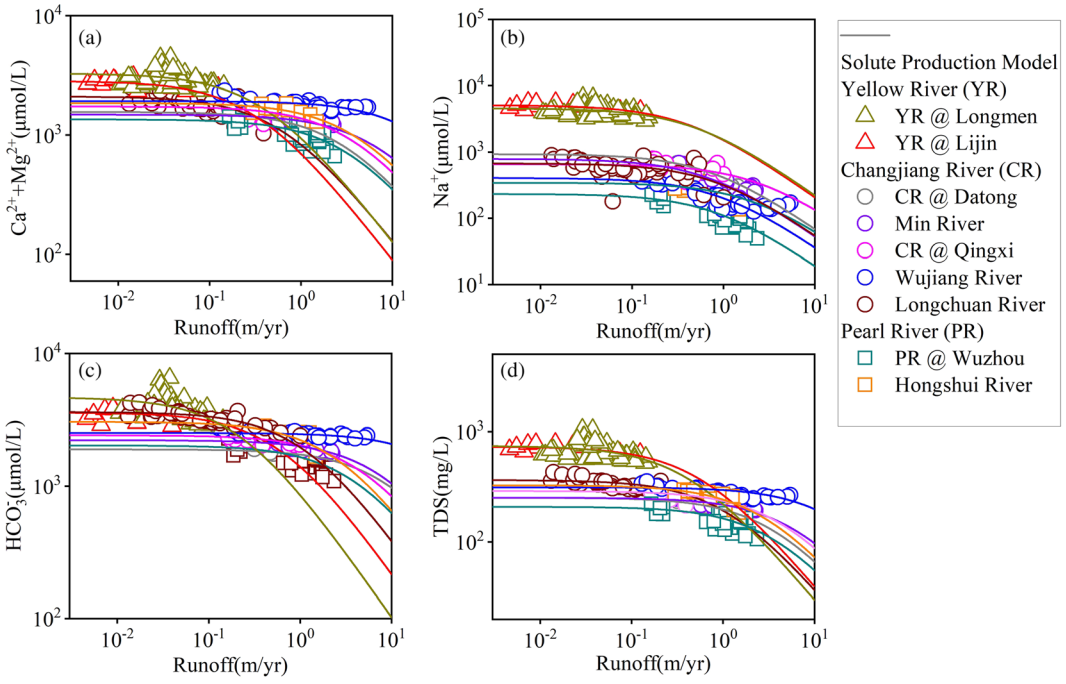

Figure 2. Concentration versus runoff for (a) Ca^{2+}, (b) Na^{+}, (c) HCO_3^{-}, and (d) TDS for Chinese monsoonal rivers, and fit of the solute production equation (Maher & Chamberlain, 2014).

Table 2
Power Law and SPM Fits for C-q Relationships in Chinese Rivers, With the Model Parameters a, b, C_{max}, and Dw

	a (μmol/L or mg/L)								*b*							
Sampling sites	Ca^{2+} +Mg^{2+}	Std	Na^{+}	Std	HCO_3^-	Std	TDS	Std	Ca^{2+} +Mg^{2+}	Std	Na^{+}	Std	HCO_3^-	Std	TDS	Std
Yellow River (YR)																
YR @ longmen	2,245	224	3,385	387	2,497	328	518	53	−0.081	0.031	−0.064	0.036	−0.133	0.040	−0.077	0.032
YR @ lijin	2,303	191	3,801	447	3,040	372	581	49	−0.041	0.020	−0.058	0.028	−0.030	0.030	−0.045	0.020
Changjiang River (CR)																
CR @ datong	1,182	18	412	20	1721	23	200	3	−0.188	0.026	−0.444	0.077	−0.078	0.026	−0.168	0.027
Min River	1,284	19	321	16	1961	12	212	2	−0.125	0.020	−0.481	0.060	−0.099	0.0088	−0.138	0.016
CR @ qingxi	1,400	72	464	62	2077	59	238	10	−0.107	0.038	−0.179	0.096	−0.072	0.021	−0.097	0.031
Wujiang River	1803	20	192	6	2,446	13	274	3	−0.082	0.010	−0.355	0.026	−0.037	0.0053	−0.086	0.011
Longchuan River	1,219	66	393	40	2,488	69	245	7	−0.149	0.018	−0.157	0.033	−0.106	0.095	−0.113	0.010
Pearl River (PR)																
PR @ wuzhou	1,029	27	106	4	1,624	40	160	4	−0.144	0.031	−0.372	0.037	−0.121	0.033	−0.144	0.033
Hongshui River	1,503	51	236	22	2,210	110	240	10	−0.131	0.047	−0.221	0.12	−0.198	0.067	−0.187	0.056

were higher than those in the CR and the PR (Table 1 and Figure 2). The *b* values of Na^{+} from power law equations were more negative than those of Ca^{2+}+Mg^{2+}, HCO_3^-, and TDS in the CR and the PR (Figure S1b and Table 2), due to a greater dilution effect of ions derived primarily from silicate weathering. The near to 0 *b* values of Ca^{2+}+Mg^{2+} and HCO_3^- were likely due to the regulation on concentrations of carbonate dissolution and precipitation (Zhong, Li, Tao, Yue, et al., 2017; Zhong et al., 2018) and near/oversaturation with respect to carbonate minerals observed in many river waters (e.g., Gaillardet et al., 2018; Ibarra et al., 2016; Zhong, Li, Tao, Yue, et al., 2017). Most of the *b* values from the YR were much closer to 0 than those from the CR and the PR (Table 2). Just from inspection of the *b* values, it is evident that these ions from the YR exhibited significant chemostatic behaviors for the present hydrologic conditions (Figure S1b and Table 2).

Power law fitting can be used to describe the solutes' behaviors but does not directly quantify reactive transport processes. The fitting of the *SPM* was employed here to capture the solute production processes responding to changing runoff (Ibarra et al., 2016; Maher & Chamberlain, 2014), which can also provide an alternative approach for parameterizing weathering processes (Ibarra et al., 2016). Derived from *SPM*, solute concentrations can be expressed as a function of *Da* (Equation 6; Figure S2). Because higher *Dw* values afford a wider range in runoff change before maximum solute flux is reached, systems with low *Dw* values exhibit stronger dilution with increasing runoff compared to catchments with high *Dw* values (Figure S2; Ibarra et al., 2016; Maher & Chamberlain, 2014). *Dw* values in YR @ Longmen and YR @ Lijin showed the lowest values for nearly all dissolved solutes (Table 2), which may be due to the arid and semiarid climate with low runoff in the YR catchment (Chen et al., 2005). For HCO_3^-, Ca^{2+}+Mg^{2+}, and TDS, *Dw* values in locations of the CR and the PR showed high values (Table 2), suggesting that stable concentrations are maintained over large runoff variations. Carbonate is widely distributed in the CR and the PR catchments, and the high *Dw* values are consistent with fast dissolution and precipitation kinetics (e.g., Gaillardet et al., 2018; Tipper et al., 2006; Zhong et al., 2018). Although *b* values of Na^{+} and TDS in the YR were near to 0, *Dw* varied in a narrow range, with low values, demonstrating that these ions showed chemostatic behaviors under the present hydrologic conditions, but might display strong dilution effects responding to future potential sustained increasing runoff.

4.2. Global Control of HCO_3^- Dynamics and Weatherability

There was a negative relationship between $HCO_3^-CV_C/CV_q$ and the average *Da* of HCO_3^- ($HCO_3^-Da_{ave}$) for global rivers (Figure 3a), suggesting that high HCO_3^--Da_{ave} induces relatively stable HCO_3^- concentrations. Fast carbonate weathering kinetics always accompany high HCO_3^--Da_{ave} values (i.e., short T_{eq}) and stable temporal HCO_3^- concentrations. We also observed a positive correlation between HCO_3^--*b* values and HCO_3^--Da_{ave} values for global rivers (Figure 3b) analyzed by Ibarra et al. (2017) and Moon et al. (2014).

Table 2
Continued

	C_{max} (μmol/L or mg/L)								*Dw* (m/yr)							
Sampling sites	$Ca^{2+}+Mg^{2+}$	Std	Na^{+}	Std	HCO_3^-	Std	TDS	Std	$Ca^{2+}+Mg^{2+}$	Std	Na^{+}	Std	HCO_3^-	Std	TDS	Std
Yellow River (YR)																
YR @ longmen	3,274	138	4,569	221	4,657	328	742	32	0.40	0.14	0.51	0.23	0.22	0.067	0.42	0.15
YR @ lijin	2,833	79	5,109	199	3,584	143	729	20	0.65	0.33	0.42	0.21	0.64	0.45	0.57	0.26
Changjiang River (CR)																
CR @ datong	1,568	63	931	132	1896	64	252	9	3.11	0.61	0.79	0.24	10.48	4.40	3.57	0.70
Min River	1,487	50	787	106	2,223	35	252	7	7.59	2.03	0.72	0.21	8.87	1.26	6.30	1.27
CR @ qingxi	1739	78	655	75	2,419	56	289	11	3.88	1.81	2.56	2.23	5.29	1.66	4.35	1.86
Wujiang River	1931	45	406	33	2,522	26	295	7	20.73	6.45	0.97	0.20	47.26	12.83	18.37	5.02
Longchuan River	2,113	58	675	34	3,616	58	364	6	1.19	0.18	0.88	0.35	1.19	0.18	1.12	0.18
Pearl River (PR)																
PR @ wuzhou	1,357	82	233	20	2028	119	208	12	3.47	0.92	0.89	0.16	4.45	1.37	3.61	0.92
Hongshui River	1,862	94	344	53	3,049	250	326	21	4.28	1.47	2.20	1.46	2.72	1.09	2.87	0.94

Both of them indicate that high HCO_3^--Da_{ave} values give rise to invariant HCO_3^- values responding to changing runoff conditions, and higher HCO_3^--Da_{ave} and HCO_3^--*b* values were observed in Chinese monsoonal rivers compared to global rivers (Figure 3b). This fast dissolution and precipitation kinetics of carbonate minerals in the weathering zone appear to dominate the inorganic carbon transport in these rivers.

Minerals with fast dissolution kinetics always have short timescales needed to approach equilibrium (Gaillardet et al., 2018; Romero-Mujalli et al., 2018; Tipper et al., 2006; Zhong et al., 2018). There are high area-normalized weathering rates in the rivers of south China, which might be caused by high reactivity (Zhong et al., 2018). Although hydrology is important during high-flow conditions due to transport limitation, thermodynamic equilibrium can also be affected by temperature (Gaillardet et al., 2018), as well as soil pCO_2 (Romero-Mujalli et al., 2018; Winnick & Maher, 2018). During the monsoon seasons, high pCO_2 from intense soil respiration, because of the wet and warm climate conditions, may also accelerate chemical weathering rates (Romero-Mujalli et al., 2018). Therefore, waters near saturation with respect to net weathering reactions result in weathering fluxes being controlled by mass transport laws rather than kinetic laws, and thus, the transit time distribution of fluids is a critical control on *WF* (Ibarra et al., 2016; Maher, 2011; Maher & Chamberlain, 2014).

The effect of HCO_3^--Da_{ave} on HCO_3^--WF_{max} was assessed in Figure 4a, revealing a positive relationship (Figure 4a). Highly affected by carbonate weathering, Chinese monsoonal rivers showed much higher HCO_3^--Da_{ave} and HCO_3^--WF_{max} values than most other global rivers (Figure 4a). We found that the

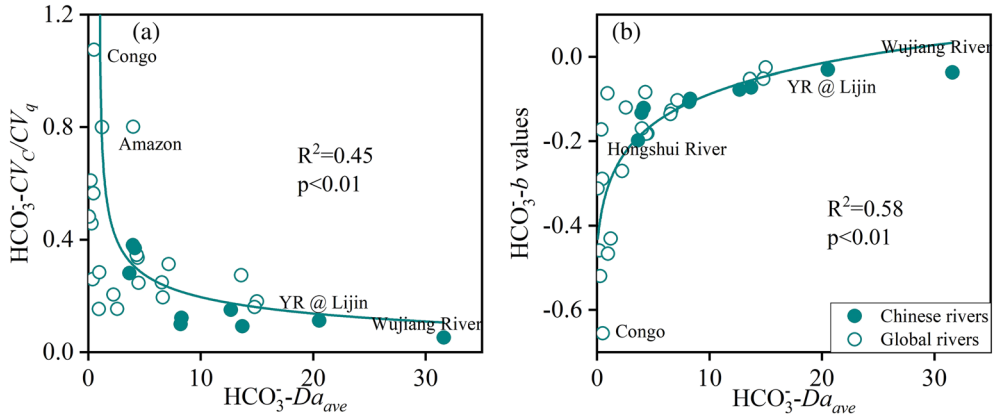

Figure 3. (a) The relationship between HCO_3^--CV_C/CV_q and HCO_3^--Da_{ave}; (b) the relationship between HCO_3^--*b* and HCO_3^--Da_{ave}. Global data were from Ibarra et al. (2017) and Moon et al. (2014).

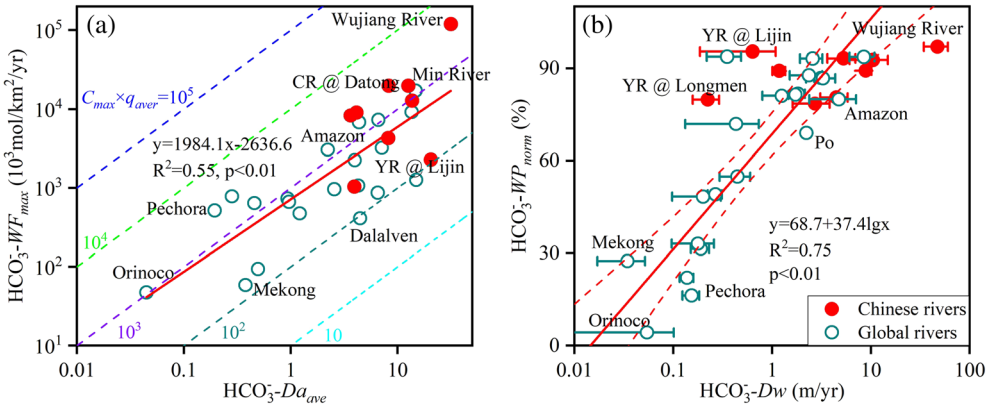

Figure 4. (a) HCO_3^--WF_{max} as a function of HCO_3^--Da_{ave}; (b) HCO_3^--WP_{norm} as a function of HCO_3^--Dw. The global data were from Ibarra et al. (2017) and Moon et al. (2014).

asymptote tended to ~10^3, with the highest $C_{max} \times q_{ave}$ values in Wujiang River (Figure 4a). Both high $(T_f)_{ave}$ and low T_{eq} would cause high HCO_3^--Da_{ave}, and high dissolution kinetics would cause low T_{eq}. Therefore, hydrologic conditions and reaction rates are the main controls on chemical weathering fluxes. Globally, HCO_3^--WF_{max} are significantly controlled by HCO_3^--Da_{ave}, and high $(T_f)_{ave}/T_{eq}$ ratios would induce high HCO_3^--WF_{max}. The positive slope of the HCO_3^--WP_{norm} and HCO_3^--Dw relationship was reported in Figure 4b and suggested that HCO_3^--WP_{norm} is highly affected by HCO_3^--Dw. Generally, rivers with high HCO_3^--Dw values produce high HCO_3^--WP_{norm}. However, because q_{ave} was much lower in the YR than most global rivers (see section 3), the HCO_3^--WP_{norm} in the YR was much higher than the average trend line of global rivers (Figure 4b).

The first factor to play a crucial role in weatherability is rock type, influencing the mineral susceptibility to weathering (Amiotte Suchet et al., 2003; Gaillardet et al., 1999; Goudie & Viles, 2012). Changes in global weatherability due to variations in runoff should be shaped by the distribution of bedrock (Ibarra et al., 2016; Torres et al., 2015; Winnick & Maher, 2018). As carbonate is dominant in the CR and PR basins compared to most global rivers, and the water chemistry of the YR is highly affected by loess distribution in the catchment, higher ion concentrations were observed in Chinese rivers than most global rivers (Gaillardet et al., 1999; Moon et al., 2014). Because of the faster dissolution kinetics compared to silicates, carbonate weathering flux has a higher sensitivity to runoff variabilities (Tipper et al., 2006; Torres et al., 2015; Zhong, Li, Tao, Yue, et al., 2017; Zhong et al., 2018). Furthermore, the CR and the YR originate from the Qinghai-Tibetan Plateau, a tectonically active region. Mountainous regions are efficient chemical weathering systems, because they result in high HCO_3^--Da_{ave} values and large discharge driven by orographic precipitation (Gaillardet et al., 2012; Maher & Chamberlain, 2014; West et al., 2005). Taken together, the climate dependence of weathering fluxes tends to be much higher in Chinese rivers than most global rivers, which we suggest is primarily due to fast dissolution kinetics.

Lithologic differences give rise to different ion concentrations in the river systems and variable weathering fluxes of the Earth's surface (Amiotte Suchet et al., 2003; Gaillardet et al., 1999; Goudie & Viles, 2012). As a peculiarity of the Earth versus other planets in the solar system (Gaillardet et al., 2018), carbonate rocks can react with biological or atmospheric CO_2, which represent a major component in global carbon cycling (Gaillardet et al., 2018; Zhong, Li, Tao, Yue, et al., 2017). The areal proportion of carbonates in these Chinese monsoonal rivers is much higher than most other global rivers (Figure 5). We find that areal proportions of carbonates had positive correlations with HCO_3^--Dw and HCO_3^--Da_{ave} (Figures 5a and 5b), which is likely due to carbonate-rich catchments having short T_{eq} for HCO_3^-. Therefore, catchments with high areal proportions of carbonates are always easy to supply HCO_3^- to the river water under changing hydrologic conditions. Positive correlations between areal proportions of carbonates and HCO_3^--WF_{max} and HCO_3^--WF_{obs} were also observed in our data set (Figures 5c and 5d), indicating that high areal proportions of carbonates induce high HCO_3^- flux globally, because of the faster dissolution kinetics of carbonate relative to silicate (Gaillardet et al., 2018; Tipper et al., 2006; Zhong, Li, Tao, Yue, et al., 2017). Chinese

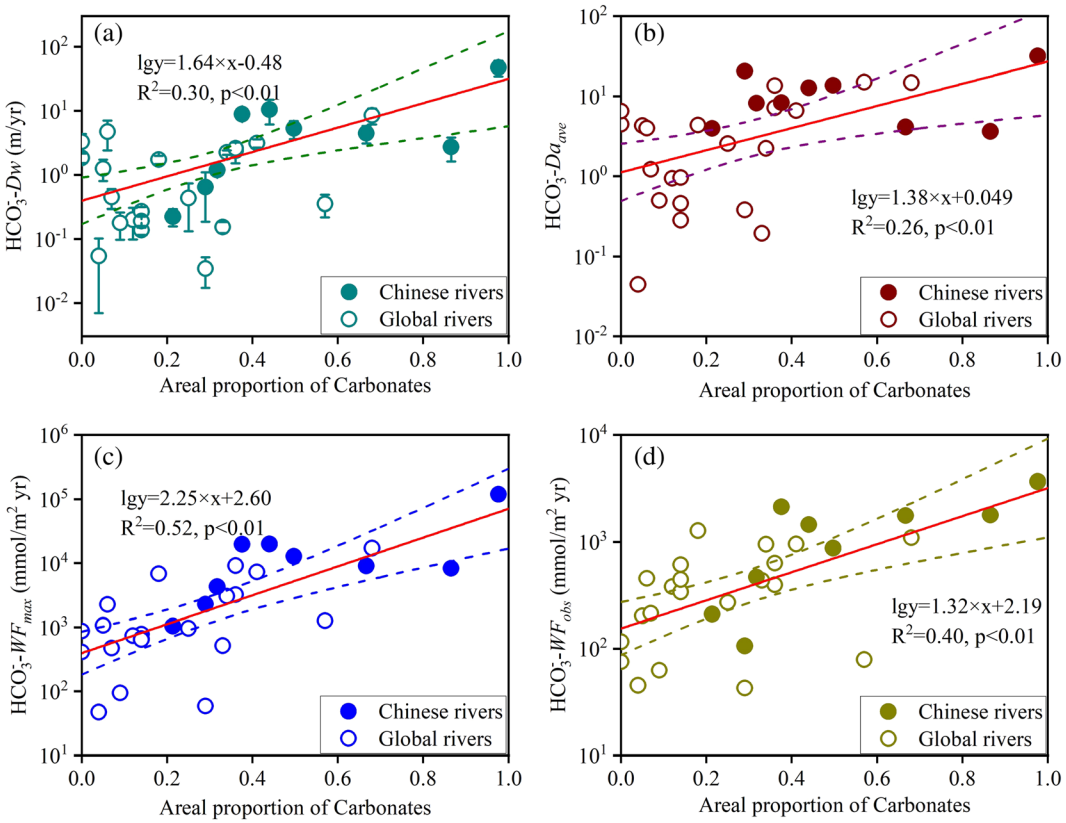

Figure 5. Areal proportion of carbonates as a function of chemical weathering. The relationship between areal proportion of carbonates and (a) HCO_3^--*Dw*, (b) HCO_3^--Da_{ave}, (c) HCO_3^--WF_{max}, and (d) HCO_3^--WF_{obs}. The areal proportion of lithologic classes of Chinese rivers were from Hartmann and Moosdorf (2012), and the areal proportion of lithologic classes and data of global rivers were from Moon et al. (2014).

monsoonal rivers in this study show stable HCO_3^- concentrations responding to changing hydrologic conditions and high area-normalized weathering rates compared to global rivers. These results confirm that globally, carbonate weathering plays a controlling role in HCO_3^- production and transport.

4.3. Implications for Quantifying Future Global Weathering Fluxes

The role of monsoonal rivers in the global weathering fluxes has important implications for understanding the feedback of global climate change on Earth surface weathering (Meyer et al., 2017; Zhong et al., 2018). Monsoonal systems delivery seasonally uneven rainfall and temperature regimes, which induce an asymmetric distribution of discharge. Intense precipitation is usually accompanied by high air temperature during the monsoonal seasons in Asia, inducing large increases in instantaneous chemical weathering rates (Li et al., 2010; Zhong et al., 2018). Because of the fast kinetics of mineral weathering in Chinese monsoonal rivers, water chemistry appears to reach equilibrium rapidly and exhibit chemostatic behaviors in response to climate variabilities up to a point (Kim et al., 2017; Zhong, Li, Tao, Yue, et al., 2017). The temporal variations of HCO_3^- concentrations in Chinese monsoonal rivers will likely be more stable than most global rivers as future river discharge increase (Pendergrass & Knutti, 2018; Figures 4a and 4b). Therefore, the solutes' fluxes will be more sensitive to hydrologic conditions in Chinese monsoonal rivers than most global rivers.

Maher and Chamberlain (2014) demonstrated that chemical weathering is controlled by hydrologic regulation, rather than directly by temperature. Although the climate model shows wide predictions, the increase in global mean temperature (*GMT*) will intensify the hydrologic cycle (increase precipitation) and result in attendant increases in runoff (Maher & Chamberlain, 2014; Manabe et al., 2004). The *GMT* sensitivities for the hydrologic cycle are 6.8%/°C, 4.8%/°C, and 3.2%/°C for high-latitude, midlatitude, and low-latitude regions, respectively (Manabe et al., 2004). Here, we used the runoff sensitivity of 4.8%/°C to estimate the

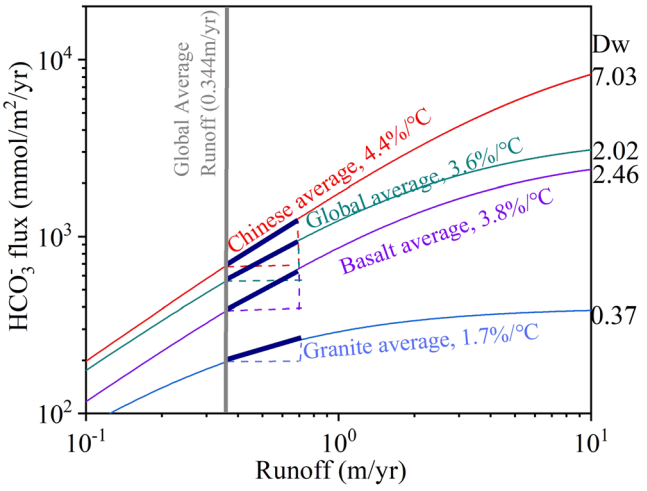

Figure 6. Sensitivity of HCO_3^- fluxes to *GMT* changes, which shows the changes in HCO_3^- fluxes for a doubling runoff at present runoff conditions. The global data were from Ibarra et al. (2017) and Moon et al. (2014), and the data sets of basalt and granite rivers were from Ibarra et al. (2016).

changes in HCO_3^- fluxes for *GMT* increase, so a doubling of runoff was associated with a *GMT* increase of 20.8°C. Although HCO_3^- fluxes were observed to be nonlinear over large temperature changes, over a small change of runoff, the percentage changes of HCO_3^- fluxes per *GMT* increase were assumed to be linear (Figure 6; Maher & Chamberlain, 2014). Based on the assumption, we calculated the *GMT* sensitivity on HCO_3^- fluxes (the percentage change in HCO_3^- flux per degree temperature increase) for present runoff conditions. The *GMT* sensitivity is 4.4%/°C for the Chinese rivers, which is much higher than the global average of 3.6%/°C (Figure 6). The high *GMT* sensitivity on HCO_3^- fluxes in Chinese rivers is due to high *Dw* values which afford large changes of runoff before achieving WF_{max}.

This *SPM* provides further insights into the sensitivity of chemical weathering to future global climate change. Under the modern ongoing global warming and attendant heavy precipitation, future climate change will induce asymmetric changes in the distribution of precipitation with disproportionately heavy rain (Pendergrass & Knutti, 2018). Because Chinese monsoonal rivers show higher *Dw* values and weathering potential than most other global rivers (Figure 4b), they will be more sensitive to the asymmetric changes in the distribution of precipitation (Pendergrass & Knutti, 2018). In other words, Chinese monsoonal rivers will play an increasingly important role in CO_2 regulation via mineral weathering for future anthropogenic climate change. This study highlights the sensitivity of short-term climate variabilities on solute production and transport in Chinese monsoonal rivers. Predicting future long-term chemical weathering and aquatic ecosystem dynamics using solute production modeling frameworks (such as the one employed in this study) will benefit understanding how changing hydrology will impact solute generation regimes in the soil-regolith weathering zone.

The strength of Earth surface weathering feedback is crucial for global carbon cycling models used for predicting future atmospheric CO_2 concentrations (Clow & Mast, 2010; Gaillardet et al., 2018; Romero-Mujalli et al., 2018) but is still highly uncertain at global scale. This study evaluated the weathering feedback patterns (i.e., *C-q* relationships) in Chinese monsoonal rivers, providing insights into the high sensitivity of weathering rates to hydrologic conditions in monsoonal regions. Moreover, additional specific studies are needed to quantify the effects of climate variabilities on Earth surface weathering in monsoonal regions globally.

5. Conclusions

This study provides insights into spatiotemporal variabilities of controlling factors on major ions in Chinese monsoonal rivers using *C-q* relationships. We showed that solute concentrations were highly affected by changing seasonal hydrologic conditions, quantified here using both power law relationships and a *SPM*. Further, variations in *C-q* relationships were regulated by ion sources and lithology among Chinese monsoonal rivers. Hydrologic flushing shaped the major ions' concentrations by changing the transit time, and the weathering intensity increased with increasing discharge, due to increasing reactive surface area. HCO_3^- in Chinese monsoonal rivers showed higher chemostatic behaviors than most global rivers due to the dominance of carbonate, and as a result weathering fluxes were more sensitive to global climate change than most other global rivers. Rock type in the Chinese monsoonal river catchments plays a primary role in weatherability and the response of weathering fluxes to hydrologic variabilities. Furthermore, Chinese monsoonal rivers will play an increasingly important role in CO_2 consumption via mineral weathering in response to global climate change over the anthropocene. Under the conditions of climate warming and attendant amplification of hydrologic cycle, Chinese rivers show much stronger sensitivity (4.4%/°C) than the global average (3.6%/°C). However, the *SPM* does not include a direct climate-biology feedback, which plays a critical role on chemical weathering. Also, it remains out of reach in the present study to separate quantitatively the effects of discharge and temperature on chemical weathering rates, both of which can affect soil pCO_2, a

critical factor in driving chemical weathering fluxes. Finally, the observations of this study emphasize the effects of runoff and thus transit times on chemical weathering to provide key insights into solute production and transport in rivers under ongoing and geologic global climate change. Future studies should be mainly focused on climate-biology feedback on chemical weathering, and the chemical weathering processes under a variety of climate conditions are also needed to better constrain climate-weathering feedback at the global scale.

Data Availability Statement

The new data analyzed in this study are available online (at https://doi.org/10.5061/dryad.fn2z34tqc), and we acknowledge Seulgi Moon for compilation of the global rivers' concentration-discharge data set from Moon et al. (2014).

Acknowledgments
This work was supported financially by National Natural Science Foundation of China (Grant 41925002), the Tianjin Science Fund for Distinguished Young Scholars (18JCJQJC46200), National Key R&D Program of China (2016YFA0601002), and the 2nd Tibetan Plateau Scientific Expedition and Research (2019QZKK0707). D. E. I. is supported by the Heising-Simons foundation, Miller Research Institute and UC President's Postdoctoral Fellowships.

References

Amiotte Suchet, P., Probst, J. L., & Ludwig, W. (2003). Worldwide distribution of continental rock lithology: Implications for the atmospheric/soil CO_2 uptake by continental weathering and alkalinity river transport to the oceans. *Global Biogeochemical Cycles*, *17*(2), 1038. https://doi.org/10.1029/2002gb001891

Baronas, J. J., Torres, M. A., Clark, K. E., & West, A. J. (2017). Mixing as a driver of temporal variations in river hydrochemistry: 2. Major and trace element concentration dynamics in the Andes-Amazon transition. *Water Resources Research*, *53*, 3120–3145. https://doi.org/10.1002/2016WR019729

Berner, R. A., & Caldeira, K. (1997). The need for mass balance and feedback in the geochemical carbon cycle. *Geology*, *25*(10), 955. https://doi.org/10.1130/0091-7613(1997)025<0955:tnfmba>2.3.co;2

Berner, R. A., Lasaga, A. C., & Garrels, R. M. (1983). The carbonate-silicate geochemical cycle and its effect on atmospheric carbon dioxide over the past 100 million years. *American Journal of Science*, *283*(7), 641–683. https://doi.org/10.2475/ajs.283.7.641

Bhatt, M. P., Hartmann, J., & Acevedo, M. F. (2018). Seasonal variations of biogeochemical matter export along the Langtang-Narayani river system in central Himalaya. *Geochimica et Cosmochimica Acta*, *238*, 208–234. https://doi.org/10.1016/j.gca.2018.06.033

Blöschl, G., & Sivapalan, M. (1995). Sale issues in hydrological modeling—A review. *Hydrological Processes*, *9*(3-4), 251–290. https://doi.org/10.1002/hyp.3360090305

Caves Rugenstein, J. K., Ibarra, D. E., & von Blanckenburg, F. (2019). Neogene cooling driven by land surface reactivity rather than increased weathering fluxes. *Nature*, *571*(7763), 99–102. https://doi.org/10.1038/s41586-019-1332-y

Chen, J., Wang, F., Meybeck, M., He, D., Xia, X., & Zhang, L. (2005). Spatial and temporal analysis of water chemistry records (1958–2000) in the Huanghe (Yellow River) basin. *Global Biogeochemical Cycles*, *19*, GB3016. https://doi.org/10.1029/2004GB002325

Clow, D. W., & Mast, M. A. (2010). Mechanisms for chemostatic behavior in catchments: Implications for CO_2 consumption by mineral weathering. *Chemical Geology*, *269*(1–2), 40–51. https://doi.org/10.1016/j.chemgeo.2009.09.014

CRAN (2018). The comprehensive R Archive Network. Accessed February 2018. https://cran.r-project.org

Dixon, J. L., Hartshorn, A. S., Heimsath, A. M., DiBiase, R. A., & Whipple, K. X. (2012). Chemical weathering response to tectonic forcing: A soils perspective from the San Gabriel Mountains, California. *Earth and Planetary Science Letters*, *323-324*, 40–49. https://doi.org/10.1016/j.epsl.2012.01.010

Gaillardet, J., Calmels, D., Romero-Mujalli, G., Zakharova, E., & Hartmann, J. (2018). Global climate control on carbonate weathering intensity. *Chemical Geology*, *527*, 118762. https://doi.org/10.1016/j.chemgeo.2018.05.009

Gaillardet, J., Dupre, B., Louvat, P., & Allegre, C. J. (1999). Global silicate weathering and CO_2 consumption rates deduced from the chemistry of large rivers. *Chemical Geology*, *159*(1–4), 3–30. https://doi.org/10.1016/S0009-2541(99)00031-5

Gaillardet, J., Rad, S., Rive, K., Louvat, P., Gorge, C., Allegre, C. J., & Lajeunesse, E. (2012). Orography-driven chemical denudation in the Lesser Antilles: Evidence for a new feed-back mechanism stabilizing atmospheric CO_2. *American Journal of Science*, *311*(10), 851–894. https://doi.org/10.2475/10.2011.02

Godsey, S. E., Kirchner, J. W., & Clow, D. W. (2009). Concentration–discharge relationships reflect chemostatic characteristics of US catchments. *Hydrological Processes*, *23*(13), 1844–1864. https://doi.org/10.1002/hyp.7315

Goudie, A. S., & Viles, H. A. (2012). Weathering and the global carbon cycle: Geomorphological perspectives. *Earth-Science Reviews*, *113*(1–2), 59–71. https://doi.org/10.1016/j.earscirev.2012.03.005

Grothendieck, G. (2013). nls2: Non-linear regression with brute force. R package version 0.2. https://cran.r-project.org/web/packages/nls2/index.html

Hartmann, J., & Moosdorf, N. (2012). The new global lithological map database GLiM: A representation of rock properties at the earth surface. *Geochemistry, Geophysics, Geosystems*, *13*, Q12004. https://doi.org/10.1029/2012GC004370

Hunsaker, C. T., & Johnson, D. W. (2017). Concentration–discharge relationships in headwater streams of the Sierra Nevada, California. *Water Resources Research*, *53*, 7869–7884. https://doi.org/10.1002/2016wr019693

Ibarra, D. E., Caves, J. K., Moon, S., Thomas, D. L., Hartmann, J., Chamberlain, C. P., & Maher, K. (2016). Differential weathering of basaltic and granitic catchments from concentration–discharge relationships. *Geochimica et Cosmochimica Acta*, *190*, 265–293. https://doi.org/10.1016/j.gca.2016.07.006

Ibarra, D. E., Moon, S., Caves, J. K., Chamberlain, C. P., & Maher, K. (2017). Concentration–discharge patterns of weathering products from global rivers. *Acta Geochimica*, *36*(3), 405–409. https://doi.org/10.1007/s11631-017-0177-z

Joesoef, A., Kirchman, D. L., Sommerfield, C. K., & Cai, W. J. (2017). Seasonal variability of the inorganic carbon system in a large coastal plain estuary. *Biogeosciences*, *14*(21), 4949–4963. https://doi.org/10.5194/bg-14-4949-2017

Kim, H., Dietrich, W. E., Thurnhoffer, B. M., Bishop, J. K. B., & Fung, I. Y. (2017). Controls on solute concentration–discharge relationships revealed by simultaneous hydrochemistry observations of hillslope runoff and stream flow: The importance of critical zone structure. *Water Resources Research*, *53*, 1424–1443. https://doi.org/10.1002/2016wr019722

Li, G. J., Hartmann, J., Derry, L. A., West, A. J., You, C. F., Long, X. Y., et al. (2016). Temperature dependence of basalt weathering. *Earth and Planetary Science Letters*, *443*, 59–69. https://doi.org/10.1016/j.epsl.2016.03.015

Li, S., Lu, X. X., He, M., Zhou, Y., Bei, R. T., Li, L., & Ziegler, A. D. (2011). Major element chemistry in the upper Yangtze River: A case study of the Longchuanjiang River. *Geomorphology*, *129*(1–2), 29–42. https://doi.org/10.1016/j.geomorph.2011.01.010

Li, S. L., Liu, C. Q., Li, J., Lang, Y. C., Ding, H., & Li, L. B. (2010). Geochemistry of dissolved inorganic carbon and carbonate weathering in a small typical karstic catchment of southwest China: Isotopic and chemical constraints. *Chemical Geology*, *277*(3–4), 301–309. https://doi.org/10.1016/j.chemgeo.2010.08.013

Liu, J., Li, S. L., Chen, J. B., Zhong, J., Yue, F. J., Lang, Y. C., & Ding, H. (2017). Temporal transport of major and trace elements in the upper reaches of the Xijiang River, SW China. *Environmental Earth Sciences*, *76*, 299. https://doi.org/10.1007/s12665-017-6625-6

Maher, K. (2010). The dependence of chemical weathering rates on fluid residence time. *Earth and Planetary Science Letters*, *294*(1–2), 101–110. https://doi.org/10.1016/j.epsl.2010.03.010

Maher, K. (2011). The role of fluid residence time and topographic scales in determining chemical fluxes from landscapes. *Earth and Planetary Science Letters*, *312*(1–2), 48–58. https://doi.org/10.1016/j.epsl.2011.09.040

Maher, K., & Chamberlain, C. P. (2014). Hydrologic regulation of chemical weathering and the geologic carbon cycle. *Science*, *343*(6178), 1502–1504. https://doi.org/10.1126/science.1250770

Manabe, S., Wetherald, R. T., Milly, P. C. D., Delworth, T. L., & Stouffer, R. J. (2004). Century-scale change in water availability: CO_2-quadrupling experiment. *Climatic Change*, *64*(1/2), 59–76. https://doi.org/10.1023/B:CLIM.0000024674.37725.ca

Meyer, K. J., Carey, A. E., & You, C. F. (2017). Typhoon impacts on chemical weathering source provenance of a high standing island watershed, Taiwan. *Geochimica et Cosmochimica Acta*, *215*, 404–420. https://doi.org/10.1016/j.gca.2017.07.015

Moon, S., Chamberlain, C. P., & Hilley, G. E. (2014). New estimates of silicate weathering rates and their uncertainties in global rivers. *Geochimica et Cosmochimica Acta*, *134*, 257–274. https://doi.org/10.1016/j.gca.2014.02.033

Musolff, A., Fleckenstein, J. H., Rao, P. S. C., & Jawitz, J. W. (2017). Emergent archetype patterns of coupled hydrologic and biogeochemical responses in catchments. *Geophysical Research Letters*, *44*, 4143–4151. https://doi.org/10.1002/2017GL072630

Pendergrass, A. G., & Knutti, R. (2018). The uneven nature of daily precipitation and its change. *Geophysical Research Letters*, *45*, 11,980–11,988. https://doi.org/10.1029/2018GL080298

Raymond, P. A. (2017). Temperature versus hydrologic controls of chemical weathering fluxes from United States forests. *Chemical Geology*, *458*, 1–13. https://doi.org/10.1016/j.chemgeo.2017.02.025

Romero-Mujalli, G., Hartmann, J., & Börker, J. (2018). Temperature and CO_2 dependency of global carbonate weathering fluxes—Implications for future carbonate weathering research. *Chemical Geology*, *527*, 118874. https://doi.org/10.1016/j.chemgeo.2018.08.010

Rose, S. (2003). Comparative solute–discharge hysteresis analysis for an urbanized and a 'control basin' in the Georgia (USA) Piedmont. *Journal of Hydrology*, *284*(1–4), 45–56. https://doi.org/10.1016/j.jhydrol.2003.07.001

Stallard, R. F., & Edmond, J. M. (1981). Geochemistry of the Amazon 1, precipitation chemistry and the marine contribution to the dissolved load at the time of peak discharge. *Journal of Geophysical Research*, *86*(C10), 9844–9858. https://doi.org/10.1029/JC086iC10p09844

Thompson, S. E., Basu, N. B., Lascurain, J., Aubeneau, A., & Rao, P. S. C. (2011). Relative dominance of hydrologic versus biogeochemical factors on solute export across impact gradients. *Water Resources Research*, *47*, WOOJ05. https://doi.org/10.1029/2010WR009605

Tipper, E. T., Bickle, M. J., Galy, A., West, A. J., Pomies, C., & Chapman, H. J. (2006). The short term climatic sensitivity of carbonate and silicate weathering fluxes: Insight from seasonal variations in river chemistry. *Geochimica et Cosmochimica Acta*, *70*(11), 2737–2754. https://doi.org/10.1016/j.gca.2006.03.005

Torres, M. A., West, A. J., & Clark, K. E. (2015). Geomorphic regime modulates hydrologic control of chemical weathering in the Andes-Amazon. *Geochimica et Cosmochimica Acta*, *166*, 105–128. https://doi.org/10.1016/j.gca.2015.06.007

von Blanckenburg, F., Bouchez, J., Ibarra, D. E., & Maher, K. (2015). Stable runoff and weathering fluxes into the oceans over quaternary climate cycles. *Nature Geoscience*, *8*(7), 538–542. https://doi.org/10.1038/NGEO2452

Walker, J. C. G., Hays, P. B., & Kasting, J. F. (1981). A negative feedback mechanism for the long-term stabilization of Earth's surface temperature. *Journal of Geophysical Research*, *86*(C10), 9776–9782. https://doi.org/10.1029/JC086iC10p09776

West, A. J. (2012). Thickness of the chemical weathering zone and implications for erosional and climatic drivers of weathering and for carbon-cycle feedbacks. *Geology*, *40*(9), 811–814. https://doi.org/10.1130/g33041.1

West, A. J., Galy, A., & Bickle, M. (2005). Tectonic and climatic controls on silicate weathering. *Earth and Planetary Science Letters*, *235*(1–2), 211–228. https://doi.org/10.1016/j.epsl.2005.03.020

Winnick, M. J., & Maher, K. (2018). Relationships between CO_2, thermodynamic limits on silicate weathering, and the strength of the silicate weathering feedback. *Earth and Planetary Science Letters*, *485*, 111–120. https://doi.org/10.1016/j.epsl.2018.01.005

Wlostowski, A. N., Gooseff, M. N., McKnight, D. M., & Lyons, W. B. (2018). Transit times and rapid chemical equilibrium explain chemostasis in glacial meltwater streams in the McMurdo Dry Valleys, Antarctica. *Geophysical Research Letters*, *45*, 13,322–13,331. https://doi.org/10.1029/2018GL080369

Wymore, A. S., Brereton, R. L., Ibarra, D. E., Maher, K., & McDowell, W. H. (2017). Critical zone structure controls concentration–discharge relationships and solute generation in forested tropical montane watersheds. *Water Resources Research*, *53*, 6279–6295. https://doi.org/10.1002/2016wr020016

Zhang, Q. Q., Jin, Z. D., Zhang, F., & Xiao, J. (2015). Seasonal variation in river water chemistry of the middle reaches of the Yellow River and its controlling factors. *Journal of Geochemical Exploration*, *156*, 101–113. https://doi.org/10.1016/j.gexplo.2015.05.008

Zhong, J., Li, S. L., Liu, J., Ding, H., Sun, X. L., Xu, S., et al. (2018). Climate variability controls on CO_2 consumption fluxes and carbon dynamics for monsoonal rivers: Evidence from Xijiang River, southwest China. *Journal of Geophysical Research: Biogeosciences*, *123*, 2553–2567. https://doi.org/10.1029/2018JG004439

Zhong, J., Li, S. L., Tao, F., Ding, H., & Liu, J. (2017). Impacts of hydrologic variations on chemical weathering and solute sources in the Min River basin, Himalayan-Tibetan region. *Environmental Science and Pollution Research*, *24*, 19,126–19,137. https://doi.org/10.1007/s11356-017-9584-2

Zhong, J., Li, S. L., Tao, F., Yue, F., & Liu, C. Q. (2017). Sensitivity of chemical weathering and dissolved carbon dynamics to hydrological conditions in a typical karst river. *Scientific Reports*, *7*, 42944. https://doi.org/10.1038/srep42944